Available online at www.sciencedirect.com
ScienceDirect
Mathematics and Computers in Simulation 185 (2021) 47–61
MATHEMATICS AND COMPUTERS IN SIMULATION
www.elsevier.com/locate/matcom

Original articles

Nonlinear dissipative slip flow of Jeffrey nanomaterial towards a curved surface with entropy generation and activation energy

M. Ijaz Khan[a,*], Faris Alzahrani[b]

[a] Department of Mathematics and Statistics, Riphah International University I-14, Islamabad 44000, Pakistan
[b] Nonlinear Analysis and Applied Mathematics (NAAM)-Research Group, Department of Mathematics, Faculty of Sciences, King Abdulaziz University, P.O. Box 80203, Jeddah 21589, Saudi Arabia

Received 4 March 2020; received in revised form 9 September 2020; accepted 4 December 2020
Available online 31 December 2020

Abstract

In this research work, mathematical modeling for steady magnetized two-dimensional (2D) incompressible flow of Jeffrey nanofluid is developed over a stretched curved surface with combined characteristics of activation energy, Brownian motion, viscous dissipation, nonlinear mixed convection, magnetohydrodynamics (MHD), Joule heating and thermophoresis diffusion. Velocity slip condition is further imposed on the curved stretched boundary. Total entropy generation rate which depends on the velocity, temperature and concentration fields is obtained via second law of thermodynamics. The dimensional differential equations are altered into dimensionless ordinary differential system by using appropriate similarity variables. The obtain system of dimensionless differential equations are solved numerically through Built-in-Shooting method. The influence of sundry flow variables associated with this problem like curvature parameter, velocity slip parameter, Deborah number, thermophoresis diffusion, Prandtl number, Brownian motion, chemical reaction, Brinkman number and activation energy are sketched for entropy generation rate, concentration, temperature and velocity field. Furthermore, Nusselt number and skin friction coefficient are calculated numerically in the presence of Deborah number, slip parameter, thermophoresis parameter, Eckert number and Brownian diffusion parameter. It is noted that velocity field is an increasing function of curvature parameter, while contrast impact is observed for Deborah number and velocity slip parameter. It is also seen that the magnitude of skin friction upsurges versus Deborah number while decays against relaxation time. Nusselt number is increased via larger Eckert number and declines against thermophoretic parameter.

Keywords: Entropy generation; Jeffrey nanofluid; Velocity slip condition; Activation energy; Viscous dissipation; Brownian and thermophoresis diffusions; Nonlinear mixed convection

1. Introduction

Nano/micro heat transport has been a significant problem for engineers and researchers in the last couple of years. The micro-devices which dimensions between 1 μm to 1 mm are effectively used in biomedical, mechanical and industrial engineering like pharmaceutical industry, electronics, automotive industries, aerospace and telecommunication to increase heat transfer rate for heating as well as cooling. The capability of heat transport can be

* Corresponding author.
E-mail address: ijazfmg_khan@yahoo.com (M.I. Khan).

https://doi.org/10.1016/j.matcom.2020.12.004

upsurged by different techniques, i.e., the utilization of vibration to heat transport surfaces, extended surfaces and the use of micro/mini-channels. On the other hand, the efficiency of heat transport can also be enhanced by increasing the transport characteristics of the working material, specifically the specific heat and thermal conductivity. The newly improved thermo-physical characteristics of working liquids are known as nanofluid or hybrid nanofluids [1–7]. By merging hybrid or nanofluids with the small channel's dimensions of the thermal tools, it is to get devices that give efficiency, compactness and low thermal resistance. The entropy generation (EG) examination is a valuable tool for execution optimization of the thermal frameworks. The EG rate could be influenced by the addition of nanoparticles in the continuous phase liquid. Therefore, the use of nanoliquids in the thermal frameworks decline the temperature of the system and the heat transport involvement to the total EG rate finally diminishes, while nanomaterial submerged into the continuous phase liquid boost the viscosity of the working liquid leads to upsurge pressure drop in the framework. Numerous analyst and investigators have examined the EG in order to minimize the rate for various thermal systems and not yet single research article is published to discuss EG in flow of Jeffrey nanofluid over a curved surface. Xie and Jian [8] studied magnetized electroosmotic flow of non-conducting viscoelastic liquid in two layer systems with entropy generation. Shah et al. [9] analyzed entropy optimized flow of ethylene glycol and aluminum nanoparticles towards a stretched surface. Ahmed at al. [10] explored unsteady entropy optimized squeezing flow with five different nanoparticles (silver, titanium oxide, water, aluminum oxide, copper oxide) between two parallel plates. Flow behavior and heat transfer rate in forced convective turbulent flow with entropy generation via isotropic permeable media is scrutinized by Torabi et al. [11]. In this problem, they used RANS models. Mathematical modeling for two-phase flow with titanium oxide and graphene oxide in the presence of entropy generation and second order velocity slip over a stretched surface is developed by Khan et al. [12]. Few more research work on entropy generation can be found in Refs. [13–20].

The development of the stretched flows in the last couple of years encouraged their fruitful implementation in different applications as in the hot rolling, rubber sheet, glass fiber, continuous casting and drawing of annealing wires, fiber spinning, melt spinning, glass blowing, cooling of huge metallic plate, polymer extrusion from a dye, paper production annealing of copper wires, wire drawing liquid crystals in condensation procedure and so forth others. The pioneer work on the development of flow over a plate surface or sheet was done by Sakiadis in 1961. The flow behavior is studied in this problem by a sheet with constant speed from a slit into a liquid at rest. The flow was of Blasius type. In 1970, Crane [21] extend the work of Sakiadis [22] by taking the plate surface is stretched and the boundary layer thickness enhanced with the distance from the slit. Heat and mass transport with blowing and suction effects by a stretching surface is discussed by Gupta and Gupta [23]. Lok et al. [24] considered non-orthogonal stagnation point flow via stretchable surface and computational results of the differential equations are found out through Keller-box method. Abel and Nandeppanavar [25] examined heat transport in magnetized flow of viscoelastic fluid towards a stretchable surface subject to non-uniform heat source/sink effect. Ishak and Pop [26] work on stagnation point flow with melting heat transport characteristics over a shrinking/stretching surface. Bao and Yang [27] explored bifurcation investigation of the stretch-twist-fold flow in generalized form. Turkyilmazoglu [28] studied flow of traditional viscoelastic (Jeffrey) Hamel fluid due to point sink or source towards a convergent/divergent channels. Si et al. [29] presented time dependent two-dimensional non-magnetized flow and heat transport of viscous liquid by a permeable stretched cylinder. Mathematical modeling for 2D steady, incompressible flow and heat transfer is developed by Mustafa et al. [30] over a stretchable rotating disk with nanomaterials. Few fruitful research work based on nanofluid can be found in Refs. [31–35].

This research work provides a comprehensive note on entropy generation (EG) in nanofluid flow towards a curved stretched surface with combined effects of activation energy, Brownian motion, viscous dissipation, nonlinear mixed convection, magnetohydrodynamics (MHD), Joule heating and thermophoresis diffusion. The nonlinear dimensional differential equations are altered into ordinary ones with the help of appropriate similarity variables. Numerical results are obtained through Built-in-Shooting method [36]. The results are compared with Sajid et al. [37] and Saif et al. [38] and found very good agreement.

2. Constitutive relations

In tensor form, the constitutive relation for Jeffrey fluid is addressed as

$$T = -pI + \tau, \tag{1}$$

where

$$p = \begin{bmatrix} p & 0 \\ 0 & p \end{bmatrix}, \tag{2}$$

$$I = \begin{bmatrix} I & 0 \\ 0 & I \end{bmatrix}, \tag{3}$$

then $-pI$ becomes

$$pI = \begin{bmatrix} p & 0 \\ 0 & p \end{bmatrix} \begin{bmatrix} I & 0 \\ 0 & I \end{bmatrix}, \tag{4}$$

$$-pI = \begin{bmatrix} -p & 0 \\ 0 & -p \end{bmatrix}. \tag{5}$$

The Cauchy stress tensor for Jeffrey fluid is defined as

$$\tau = \begin{bmatrix} \tau_{rr} & \tau_{rs} \\ \tau_{sr} & \tau_{ss} \end{bmatrix} = \frac{1}{1+\lambda_1}\left[\mathbf{A}_1 + \lambda_2 \dot{\mathbf{A}}_1\right], \tag{6}$$

where $\dot{\mathbf{A}}$ is addressed as

$$\mathbf{A}_1 = \mathbf{L} + \mathbf{L}^T. \tag{7}$$

In Eq. (7), $\mathbf{L}$ and $\mathbf{L}^T$ are mathematically defined as

$$\mathbf{L} = \text{grad}\,\mathbf{V} = \begin{bmatrix} \frac{\partial v}{\partial r} & \frac{-uR}{r+R} \\ \frac{\partial u}{\partial r} & \frac{vR}{r+R} + \frac{R}{r+R}\frac{\partial u}{\partial s} \end{bmatrix}, \tag{8}$$

$$\mathbf{L}^T = (\text{grad}\,\mathbf{V})^T = \begin{bmatrix} \frac{\partial v}{\partial r} & \frac{\partial u}{\partial r} \\ \frac{-uR}{r+R}\frac{\partial u}{\partial r} & \frac{vR}{r+R} + \frac{R}{r+R}\frac{\partial u}{\partial s} \end{bmatrix}. \tag{9}$$

Invoking Eqs. (8) and (9) in Eq. (7), we arrive

$$\mathbf{A}_1 = \begin{bmatrix} \frac{\partial v}{\partial r} & \frac{-uR}{r+R} \\ \frac{\partial u}{\partial r} & \frac{vR}{r+R} + \frac{R}{r+R}\frac{\partial u}{\partial s} \end{bmatrix} + \begin{bmatrix} \frac{\partial v}{\partial r} & \frac{\partial u}{\partial r} \\ \frac{-uR}{r+R}\frac{\partial u}{\partial r} & \frac{vR}{r+R} + \frac{R}{r+R}\frac{\partial u}{\partial s} \end{bmatrix}. \tag{10}$$

Put Eq. (10) in Eq. (6), one has

$$\tau_{rr} = \frac{2\mu}{1+\lambda_1}\left[1 + \lambda_2\left(v\frac{\partial}{\partial r} + \frac{Ru}{r+R}\frac{\partial}{\partial s}\right)\right]\frac{\partial v}{\partial s}, \tag{11}$$

$$\tau_{rs} = \frac{\mu}{1+\lambda_1}\left[1 + \lambda_2\left(v\frac{\partial}{\partial r} + \frac{Ru}{r+R}\frac{\partial}{\partial s}\right)\right]\left[\frac{\partial u}{\partial r} + \frac{R}{r+R}\frac{\partial v}{\partial s} - \frac{u}{r+R}\right], \tag{12}$$

$$\tau_{ss} = \frac{2\mu}{1+\lambda_1}\left[1 + \lambda_2\left(v\frac{\partial}{\partial r} + \frac{Ru}{r+R}\frac{\partial}{\partial s}\right)\right]\left[\frac{R}{r+R}\frac{\partial u}{\partial s} + \frac{v}{r+R}\right]. \tag{13}$$

In the above equations T, p, τ, λ_1, λ_2, $\mathbf{A}_1$, $\dot{\mathbf{A}}_1$ represent Cauchy stress tensor, pressure, extra stress tensor, ratio of relaxation to retardation time, retardation time, first Rivlin–Erickson tensor and material time derivative respectively.

3. Statement

Here magnetized steady 2D incompressible flow of non-Newtonian fluid (Jeffrey fluid) is considered towards a curved surface. Flow is generated due to curved stretched surface. The flow is electrical conducting through applied magnetic field of strength B_0. Nonlinear mixed convection is considered. The mixed convection occurs when both forced and natural convections act together in a fluid to transfer heat. It is also addressed as in the literature where both buoyant and pressure forces act together. Brownian and thermophoretic effects are

studied by nanofluid. Entropy minimization and Bejan number is further studied. Velocity slip is accounted for boundary condition of momentum equation and nonlinear mixed convection is established in velocity equation. Heat and mass transfer is studied with additional effect of viscous dissipation and activation energy respectively. Flow is along $r-$direction and sheet is stretched along $s-$direction. In the boundary conditions $u = U_w = as + \frac{\gamma_1}{1+\lambda_1}\left[1+\lambda_2\left(v\frac{\partial}{\partial r}+\frac{Ru}{r+R}\frac{\partial}{\partial s}\right)\right]\left[\frac{\partial u}{\partial r}+\frac{R}{r+R}\frac{\partial v}{\partial s}-\frac{u}{r+R}\right]$ represents the stretching velocity along with first order velocity, $v = 0$ means there is no suction/injection at the curved surface, $T_w, C_w, T_\infty, C_\infty$ highlight the wall as well as ambient temperature and concentration respectively. Governing equations for Jeffrey model subject to nonlinear mixed convection, magnetohydrodynamics, activation energy, Brownian motion, viscous dissipation, chemical reaction, thermophoresis diffusion and Joule heating are in tensor form are addressed as [39,40]:

$$\frac{\partial}{\partial r}\left[(r+R)v\right]+R\frac{\partial u}{\partial s}=0, \tag{14}$$

$$\rho\left(v\frac{\partial v}{\partial r}+\frac{Ru}{r+R}\frac{\partial v}{\partial s}-\frac{u^2}{r+R}\right)=-\frac{\partial p}{\partial r}-\frac{\tau_{ss}}{r+R}+\frac{R}{r+R}\frac{\partial \tau_{sr}}{\partial r}+\frac{1}{r+R}\frac{\partial}{\partial r}\left[(r+R)\tau_{rr}\right], \tag{15}$$

$$\left.\begin{aligned}\rho\left(u\tfrac{\partial u}{\partial r}+\tfrac{Ru}{r+R}\tfrac{\partial u}{\partial s}+\tfrac{uv}{r+R}\right)&=-\tfrac{R}{r+R}\tfrac{\partial p}{\partial s}+\tfrac{R}{r+R}\tfrac{\partial \tau_{ss}}{\partial s}+\tfrac{1}{(r+R)^2}\tfrac{\partial}{\partial r}\left[(r+R)^2\tau_{rs}\right]\\ -\sigma B_0^2u+g\rho\left(\beta_1\left(T-T_\infty\right)+\beta_2\left(T-T_\infty\right)^2+\beta_3\left(C-C_\infty\right)+\beta_4\left(C-C_\infty\right)^2\right),&\end{aligned}\right\} \tag{16}$$

$$\left.\begin{aligned}v\tfrac{\partial T}{\partial r}+\tfrac{\partial T}{\partial s}\tfrac{uR}{R+r}&=\tfrac{k}{\left(\rho c_p\right)_f}\left(\tfrac{\partial^2 T}{\partial r^2}+\tfrac{\partial T}{\partial r}\tfrac{1}{R+r}\right)+S:L+\tfrac{\sigma}{\left(\rho c_p\right)_f}B_0^2u^2\\ &+\tfrac{\left(\rho c_p\right)_s}{\left(\rho c_p\right)_f}\left(\tfrac{D_T}{T_\infty}\left(\tfrac{\partial T}{\partial r}\right)^2+D_B\tfrac{\partial C}{\partial r}\tfrac{\partial T}{\partial r}\right),\end{aligned}\right\} \tag{17}$$

$$\left.\begin{aligned}v\tfrac{\partial C}{\partial r}+\tfrac{\partial C}{\partial s}\tfrac{uR}{R+r}&=D_B\left(\tfrac{\partial^2 C}{\partial r^2}+\tfrac{\partial C}{\partial r}\tfrac{1}{R+r}\right)+\tfrac{D_T}{T_\infty}\left(\tfrac{\partial^2 T}{\partial r^2}+\tfrac{\partial T}{\partial r}\tfrac{1}{R+r}\right)\\ &-k_r^2\left(C-C_\infty\right)\left(\tfrac{T}{T_\infty}\right)^n\exp\left[\tfrac{-E_a}{\kappa T}\right],\end{aligned}\right\} \tag{18}$$

where (u, v), (r, s), ρ, R, σ, B_0, T, k, $\left(\rho c_p\right)_f$, $\left(\rho c_p\right)_p$, $S : L$, D_T, T_∞, D_B, C, k_r, C_∞, $n = [-1, 1]$, E_a, $\kappa = 5.67 \times 10^{-5}$ eV/K highlight the velocities, curvilinear coordinates, density, radius, electrical conductivity, strength of magnetic field, temperature, thermal conductivity, heat capacity of fluid, heat capacity of solid, the viscous dissipation, the coefficient of thermophoretic, ambient temperature, Brownian diffusion coefficient, concentration, chemical reaction rate, ambient concentration, the fitted rate constant, activation energy and Stefan Boltzmann constant respectively. Here $S : L$ is addressed as

$$S:L=\frac{\mu}{1+\lambda_1}\left[\left(\frac{\partial u}{\partial r}\right)^2-\frac{u}{r+R}\frac{\partial u}{\partial r}+\left(\frac{u}{r+R}\right)^2+\lambda_2\left(\begin{array}{c}\frac{uv}{r+R}\frac{\partial^2 u}{\partial r^2}+\frac{uv}{(r+R)^2}\frac{\partial u}{\partial r}-\frac{u^2v}{(r+R)^3}\\ -\frac{Ru^2}{(r+R)^2}\frac{\partial^2 u}{\partial r\partial s}+\frac{u^2R}{(r+R)^3}\frac{\partial u}{\partial s}+v\frac{\partial u}{\partial r}\frac{\partial^2 u}{\partial r^2}\\ -\frac{v}{r+R}\left(\frac{\partial u}{\partial r}\right)^2+\frac{uv}{(r+R)^2}\frac{\partial u}{\partial r}-\frac{uR}{(r+R)^2}\frac{\partial u}{\partial r}\frac{\partial u}{\partial s}\end{array}\right)\right], \tag{19}$$

After putting extra stress tensors final form of equations become

$$\begin{aligned}\rho\left(v\frac{\partial v}{\partial r}+\frac{uR}{r+R}\frac{\partial v}{\partial s}-\frac{u^2}{r+R}\right)&=-\frac{\partial p}{\partial r}+\frac{\mu}{1+\lambda_1}\left[2\frac{\partial^2 v}{\partial r\partial s}+\frac{2}{r+R}\frac{\partial v}{\partial s}+\frac{R}{r+R}\frac{\partial^2 u}{\partial r^2}-\frac{R^2}{(r+R)^3}\frac{\partial v}{\partial s}\right.\\ &+\left(\frac{R}{r+R}\right)^2\frac{\partial^2 v}{\partial r\partial s}+\frac{Ru}{(r+R)^3}-\frac{R}{(r+R)^2}\frac{\partial u}{\partial r}-\frac{2R}{(r+R)^2}\frac{\partial u}{\partial s}\\ &-\frac{2v}{(r+R)^2}+\lambda_2\left(\frac{2R}{r+R}\frac{\partial^2 v}{\partial s^2}\frac{\partial u}{\partial r}-\frac{2R}{(r+R)^2}u\frac{\partial^2 v}{\partial s^2}+\frac{2R}{r+R}u\frac{\partial^3 v}{\partial r\partial s^2}\right.\\ &+2\frac{\partial v}{\partial r}\frac{\partial^2 v}{\partial r\partial s}+2v\frac{\partial^3 v}{\partial r^2\partial s}+\frac{2uR}{r+R}\frac{\partial^2 v}{\partial s^2}+2v\frac{\partial^2 v}{\partial r\partial s}-\frac{R^2u}{(r+R)^3}\frac{\partial^2 u}{\partial r\partial s}\\ &\left.\left.+\frac{R^2}{(r+R)^2}\frac{\partial u}{\partial r}\frac{\partial^2 u}{\partial r\partial s}+\frac{R^2u}{(r+R)^2}\frac{\partial^3 v}{\partial r^2\partial s}+\frac{R^3u}{(r+R)^3}\frac{\partial^3 v}{\partial r\partial s^2}\right)\right]\end{aligned}$$

$$+\frac{R^3}{(r+R)^3}\frac{\partial u}{\partial r}\frac{\partial^2 v}{\partial s^2}-\frac{2R^3u}{(r+R)^4}\frac{\partial^2 v}{\partial s^2}+\frac{2R^2u}{(r+R)^4}\frac{\partial u}{\partial s}-\frac{R^2}{(r+R)^3}\frac{\partial u}{\partial r}\frac{\partial u}{\partial s}$$
$$-\frac{Ru}{(r+R)^2}\frac{\partial^2 u}{\partial r\partial s}+\frac{R}{r+R}\frac{\partial v}{\partial r}\frac{\partial^2 u}{\partial r^2}+\frac{Rv}{r+R}\frac{\partial^3 u}{\partial r^3}-\frac{R^2}{(r+R)^3}\frac{\partial v}{\partial r}\frac{\partial v}{\partial s}$$
$$-\frac{2R^2v}{(r+R)^3}\frac{\partial^2 v}{\partial r\partial s}+\frac{2vR^2}{(r+R)^4}\frac{\partial v}{\partial s}+\frac{R^2}{(r+R)^2}\frac{\partial v}{\partial r}\frac{\partial^2 v}{\partial r\partial s}+\frac{R^2v}{(r+R)^2}\frac{\partial^3 v}{\partial r^2\partial s}$$
$$+\frac{2Rv}{(r+R)^3}\frac{\partial u}{\partial r}+\frac{Ru}{(r+R)^3}\frac{\partial v}{\partial r}-\frac{2Ruv}{(r+R)^4}-\frac{R}{(r+R)^2}\frac{\partial v}{\partial r}\frac{\partial u}{\partial r}$$
$$-\frac{2R^2u}{(r+R)^3}\frac{\partial^2 u}{\partial s^2}-\frac{2Ru}{(r+R)^3}\frac{\partial v}{\partial s}+\frac{2vR}{(r+R)^3}\frac{\partial u}{\partial s}-\frac{2vR}{(r+R)^2}\frac{\partial^2 u}{\partial r\partial s}$$
$$+\frac{2v^2}{(r+R)^3}-\frac{Rv}{(r+R)^2}\frac{\partial^2 u}{\partial r^2}-\frac{2v}{(r+R)^2}\frac{\partial v}{\partial r}\Bigg)\Bigg], \tag{20}$$

$$\rho\left(v\frac{\partial u}{\partial r}+\frac{uR}{r+R}\frac{\partial u}{\partial s}+\frac{uv}{r+R}\right)=-\frac{R}{r+R}\frac{\partial p}{\partial s}+\frac{\mu}{1+\lambda_1}\left[\frac{2R^2}{(r+R)^2}\frac{\partial^2 u}{\partial s^2}+\frac{\partial^2 u}{\partial r^2}+\frac{R}{r+R}\frac{\partial^2 v}{\partial s\partial r}\right.$$
$$+\frac{1}{r+R}\frac{\partial u}{\partial r}+\frac{3R}{(r+R)^2}\frac{\partial v}{\partial s}-\frac{u}{(r+R)^2}+\lambda_2\left(\frac{2R^3}{(r+R)^3}\frac{\partial u}{\partial s}\frac{\partial^2 u}{\partial s^2}\right.$$
$$+\frac{2R^3u}{(r+R)^3}\frac{\partial^3 u}{\partial s^3}+\frac{4R^2u}{(r+R)^3}\frac{\partial^2 v}{\partial s^2}-\frac{2R^2v}{(r+R)^3}\frac{\partial^2 u}{\partial s^2}+\frac{2R^2}{(r+R)^3}\frac{\partial v}{\partial s}\frac{\partial^2 u}{\partial s\partial r}$$
$$+\frac{2R^2v}{(r+R)^3}\frac{\partial^3 u}{\partial r\partial s^2}-\frac{4Rv}{(r+R)^3}\frac{\partial v}{\partial s}+\frac{2R}{(r+R)^2}\left(\frac{\partial v}{\partial s}\right)^2+\frac{Rv}{(r+R)^2}\frac{\partial^2 v}{\partial r\partial s}$$
$$+\frac{R}{r+R}\frac{\partial u}{\partial r}\frac{\partial^2 u}{\partial r\partial s}+\frac{Ru}{(r+R)}\frac{\partial^3 u}{\partial r^2\partial s}+\frac{R^2}{(r+R)^2}\frac{\partial^2 v}{\partial s^2}\frac{\partial u}{\partial r}+\frac{Rv}{(r+R)^2}\frac{\partial^2 v}{\partial r\partial s}$$
$$+\frac{R^2u}{(r+R)^2}\frac{\partial^3 v}{\partial r\partial s^2}-\frac{2R^2u}{(r+R)^3}\frac{\partial^2 u}{\partial s^2}-\frac{R}{(r+R)^2}\frac{\partial u}{\partial s}\frac{\partial u}{\partial r}+\frac{\partial v}{\partial r}\frac{\partial^2 u}{\partial r^2}+v\frac{\partial^3 u}{\partial r^3}$$
$$-\frac{R}{(r+R)^2}\frac{\partial v}{\partial s}\frac{\partial v}{\partial r}+\frac{R}{r+R}\frac{\partial v}{\partial r}\frac{\partial^2 v}{\partial r\partial s}+\frac{Rv}{r+R}\frac{\partial^3 v}{\partial r^2\partial s}+\frac{u}{(r+R)^2}\frac{\partial v}{\partial r}$$
$$\left.\left.-\frac{1}{r+R}\frac{\partial u}{\partial r}\frac{\partial v}{\partial r}+\frac{v}{(r+R)}\frac{\partial^2 u}{\partial r^2}\right)\right]-\sigma B_0^2u$$
$$+g\rho\left(\beta_1(T-T_\infty)+\beta_2(T-T_\infty)^2+\beta_3(C-C_\infty)+\beta_4(C-C_\infty)^2\right), \tag{21}$$

$$\left.\begin{aligned} v\tfrac{\partial T}{\partial r}+\tfrac{\partial t}{\partial s}\tfrac{uR}{R+r}&=\tfrac{k}{(\rho c_p)_f}\left(\tfrac{\partial^2 T}{\partial r^2}+\tfrac{\partial T}{\partial r}\tfrac{1}{R+r}\right)+\tfrac{(\rho c_p)_s}{(\rho c_p)_f}\left(\tfrac{D_T}{T_\infty}\left(\tfrac{\partial T}{\partial r}\right)^2+D_B\tfrac{\partial C}{\partial r}\tfrac{\partial T}{\partial r}\right)+\tfrac{\sigma}{(\rho c_p)_f}B_0^2u^2,\\ +\tfrac{\mu}{1+\lambda_1}&\left[\left(\tfrac{\partial u}{\partial r}\right)^2-\tfrac{u}{r+R}\tfrac{\partial u}{\partial r}+\left(\tfrac{u}{r+R}\right)^2+\lambda_2\left(\begin{array}{c}\tfrac{uv}{r+R}\tfrac{\partial^2 u}{\partial r^2}+\tfrac{uv}{(r+R)^2}\tfrac{\partial u}{\partial r}-\tfrac{u^2v}{(r+R)^3}\\ -\tfrac{Ru^2}{(r+R)^2}\tfrac{\partial^2 u}{\partial r\partial s}+\tfrac{u^2R}{(r+R)^3}\tfrac{\partial u}{\partial s}+v\tfrac{\partial u}{\partial r}\tfrac{\partial^2 u}{\partial r^2}\\ -\tfrac{v}{r+R}\left(\tfrac{\partial u}{\partial r}\right)^2+\tfrac{uv}{(r+R)^2}\tfrac{\partial u}{\partial r}-\tfrac{uR}{(r+R)^2}\tfrac{\partial u}{\partial r}\tfrac{\partial u}{\partial s}\end{array}\right)\right] \end{aligned}\right\}, \tag{22}$$

$$\left.\begin{aligned} v\tfrac{\partial C}{\partial r}+\tfrac{\partial C}{\partial s}\tfrac{uR}{R+r}&=D_B\left(\tfrac{\partial^2 C}{\partial r^2}+\tfrac{\partial C}{\partial r}\tfrac{1}{R+r}\right)+\tfrac{D_T}{T_\infty}\left(\tfrac{\partial^2 T}{\partial r^2}+\tfrac{\partial T}{\partial r}\tfrac{1}{R+r}\right)\\ &-k_r^2(C-C_\infty)\left(\tfrac{T}{T_\infty}\right)^n\exp\left[\tfrac{-E_a}{\kappa T}\right], \end{aligned}\right\} \tag{23}$$

Finally, implementing the technique [41] and boundary layer concept [42], we arrive to the following differential system

$$\frac{\partial}{\partial r}\{(r+R)v\}+R\frac{\partial u}{\partial s}=0, \tag{24}$$

$$\frac{\rho u^2}{r+R} = \frac{\partial p}{\partial r}, \tag{25}$$

$$\left.\begin{array}{c} \rho\left(v\frac{\partial u}{\partial r} + \frac{uR}{r+R}\frac{\partial u}{\partial s} + \frac{uv}{r+R}\right) = -\frac{R}{r+R}\frac{\partial p}{\partial s} - \sigma B_0^2 u \\ +g\rho\left(\beta_1 (T-T_\infty) + \beta_2 (T-T_\infty)^2 + \beta_3 (C-C_\infty) + \beta_4 (C-C_\infty)^2\right) \\ +\frac{\mu}{1+\lambda_1}\left[\begin{array}{c} \frac{\partial^2 u}{\partial r^2} + \frac{1}{r+R}\frac{\partial u}{\partial r} + \frac{2R}{(r+R)^2}\frac{\partial v}{\partial s} - \frac{u}{(r+R)^2} \\ +\lambda_2\left(\begin{array}{c} \frac{R}{r+R}\frac{\partial u}{\partial r}\frac{\partial^2 u}{\partial r \partial s} + \frac{Ru}{(r+R)}\frac{\partial^3 u}{\partial r^2 \partial s} - \frac{R}{(r+R)^2}\frac{\partial u}{\partial s}\frac{\partial u}{\partial r} + \frac{\partial v}{\partial r}\frac{\partial^2 u}{\partial r^2} \\ +v\frac{\partial^3 u}{\partial r^3} + \frac{u}{(r+R)^2}\frac{\partial v}{\partial r} - \frac{1}{r+R}\frac{\partial u}{\partial r}\frac{\partial v}{\partial r} + \frac{v}{(r+R)}\frac{\partial^2 u}{\partial r^2} \end{array}\right) \end{array}\right] \end{array}\right\} \tag{26}$$

with

$$\left.\begin{array}{c} u = U_w = as + \frac{\gamma_1}{1+\lambda_1}\left[1 + \lambda_2\left(v\frac{\partial}{\partial r} + \frac{Ru}{r+R}\frac{\partial}{\partial s}\right)\right]\left[\frac{\partial u}{\partial r} + \frac{R}{r+R}\frac{\partial v}{\partial s} - \frac{u}{r+R}\right], \\ v = 0, \quad T = T_w, \ C = C_w \ \text{ at } r = 0, \\ u \to 0, \quad \frac{\partial u}{\partial r} \to 0, \quad T \to T_\infty, \ C \to C_\infty \ \text{ at } r \to \infty. \end{array}\right\} \tag{27}$$

Let

$$u = asf'(\xi), \quad v = \frac{-R}{r+R}\sqrt{a\nu}f(\xi), \ \xi = \sqrt{\frac{a}{\nu}}r, \quad p = \rho a^2 s^2 P(\xi), \quad \theta = \frac{T-T_\infty}{T_w - T_\infty}. \tag{28}$$

The above system is altered into the following ordinary differential system

$$P' = \frac{f'^2}{\xi + K}, \tag{29}$$

$$\left.\begin{array}{c} 2P = ff'' - f'^2 + \frac{ff'}{\xi+K} - Mf' + \frac{1}{1+\lambda_1}\left[\begin{array}{c} f'''\frac{\xi+K}{K} + \frac{1}{K}f'' - \frac{1}{K(\xi+K)}f' \\ +\beta\left(f''^2 - \frac{1}{(\xi+K)^2}f'^2 - ff^{iv} + \frac{1}{(\xi+K)^3}ff' - \frac{1}{(\xi+K)^2}ff''\right) \end{array}\right] \end{array}\right\}$$
$$+\lambda^*\theta(1+\beta_t\theta) + \lambda^* N^*\phi\,(1+\beta_c\phi)\,, \tag{30}$$

$$\frac{1}{\mathrm{Pr}}\left(\theta'' + \frac{\theta'}{\xi+K}\right) + \frac{K}{\xi+K}f\theta' + Nt\theta'^2 + Nb\theta'\phi' + MEcf'^2$$
$$+\frac{Ec}{1+\lambda_1}\left(\begin{array}{c} f'' - \frac{1}{\xi+K}f'f'' + \frac{f'^2}{(\xi+K)^2} \\ +\beta\left(\begin{array}{c} -\frac{A}{(\xi+K)^2}ff' - \frac{A}{(\xi+K)^3}ff'f'' + ff'^2\frac{A}{(\xi+K)^4} \\ -\frac{A}{(\xi+K)^2}f'^2f'' + f'^3\frac{A}{(\xi+K)^3} \end{array}\right) \end{array}\right) = 0, \tag{31}$$

$$\phi'' + \frac{1}{\xi+K}\phi' + \frac{A}{\xi+K}Scf\phi' + \frac{Nt}{Nb}\left(\theta'' + \frac{1}{\xi+K}\theta'\right) - k_1 Sc(1+\alpha_1\theta)\phi\exp\left[\frac{-E_1}{1+\alpha_1\phi}\right] = 0, \tag{32}$$

with

$$\left.\begin{array}{c} f(0) = 0, \ f'(0) = 1 + \frac{L_1}{1+\lambda_1}\left[f''(0) - \frac{f'(0)}{K} + \beta\left(f'(0)f''(0) - \frac{1}{K}(f'(0))^2\right)\right], \\ f'(\infty) = 0, \ f''(\infty) = 0, \ \theta(0) = 1, \ \theta(\infty) = 0, \phi(0) = 1, \ \phi(\infty) = 0. \end{array}\right\} \tag{33}$$

where K, L_1, M, β, Pr, Nt, Ec, Nb, Sc, λ^*, β_t, β_c, N^*, k_1, α_1, E_1 show the curvature parameter, slip parameter, magnetic parameter, Deborah number, Prandtl number, thermophoretic parameter, Eckert number, Brownian diffusion parameter, Schmidt number, mixed convection parameter, nonlinear thermal and solutal mixed convection parameters, ratio of buoyancy forces, reaction parameter, temperature difference parameter and activation

energy parameter respectively. These parameters are defined as

$$\left.\begin{aligned} K=\sqrt{\tfrac{a}{\nu}}R,\ L_1=\gamma_1\sqrt{\tfrac{a}{\nu}}, M=\tfrac{\sigma B_0^2}{\rho a},\ \beta=\lambda_2 a,\ \mathrm{Pr}=\tfrac{(\rho c_p)_f \nu}{k},\ Nt=\tfrac{(\rho c_p)_s D_T (T_w-T_\infty)}{(\rho c_p)_f \nu T_\infty},\\ Ec=\tfrac{a^2 s^2}{c_p(T_w-T_\infty)},\ \ Nb=\tfrac{(\rho c_p)_s D_B (C_w-C_\infty)}{(\rho c_p)_f \nu},\ \ Sc=\tfrac{D_B}{\nu},\ \ \lambda^*=\tfrac{g\beta_1(T_w-T_\infty)s^3}{\nu_f^2}\\ \beta_t=\tfrac{\beta_2(T_w-T_\infty)}{\beta_1},\ \ \beta_c=\tfrac{\beta_4(C_w-C_\infty)}{\beta_3}, N^*=\tfrac{\beta_3(C_w-C_\infty)}{\beta_1(T_w-T_\infty)}, k_1=\tfrac{k_r^2}{a},\\ \alpha_1=\tfrac{T_w-T_\infty}{T_w},\ \ E_1=\tfrac{E_a}{\kappa T_\infty}. \end{aligned}\right\} \tag{34}$$

For omission of pressure term, we have taken derivative of Eq. (30) and put it in Eq. (29), one has

$$\left.\begin{aligned} f^{iv}(\xi+K)^5+2(\xi+K)^4 f'''+(\xi+K)^2 f'-(\xi+K)^3 f''+\beta K(2(\xi+K)^4 f'' f'''\\ -(\xi+K)^4 f f^v-(\xi+K)^4 f' f^{iv}+3(\xi+K)f'^2+3(\xi+K)ff''-3(\xi+K)^2 f' f''\\ -3(\xi+K)^2 ff'''-3ff')+(1+\lambda_1)K((\xi+K)^4 ff'''-(\xi+K)^4 f' f''-(\xi+K)^2 ff'\\ -(\xi+K)^3 f'^2+(\xi+K)^3 ff''-M\left((\xi+K)^5 f''+(\xi+K)^4 f'\right)\\ +(\xi+K)^5\left(\lambda^*\theta'+2\lambda^*\theta\theta'\beta_t+\lambda^* N^*\phi'+2\lambda^* N^*\beta_c\phi\phi'\right))=0, \end{aligned}\right\} \tag{35}$$

Form Eq. (30), we can also find the pressure

$$\left.\begin{aligned} P=\tfrac{1}{2}\left(ff''-f'^2+\tfrac{ff'}{\zeta+K}\right)+\tfrac{1}{2(1+\lambda_1)}\left[\begin{array}{c} f'''\tfrac{\xi+K}{K}+\tfrac{1}{K}f''-\tfrac{1}{K(\xi+K)}f'\\ +\lambda_2\left(\begin{array}{c} f''^2-\tfrac{1}{(\xi+K)^2}f'^2-ff^{iv}\\ +\tfrac{1}{(\xi+K)^3}ff'-\tfrac{1}{(\xi+K)^2}ff'' \end{array}\right) \end{array}\right]\\ -Mf'+\lambda^*\theta(1+\beta_t\theta)+\lambda^* N^*\phi\,(1+\beta_c\phi) \end{aligned}\right\}. \tag{36}$$

4. Engineering interest

The engineering quantities like skin friction is defined as

$$\left.\begin{aligned} C_{fs}=\tfrac{\tau_{rs}}{\frac{\rho}{2}U_w^2},\\ Nu_x=\tfrac{sq_w}{k(T_w-T_\infty)}, \end{aligned}\right\} \tag{37}$$

where

$$\left.\begin{aligned} \tau_{rs}=\tfrac{\mu}{1+\lambda_1}\left[1+\lambda_2\left(v\tfrac{\partial}{\partial r}+\tfrac{Ru}{r+R}\tfrac{\partial}{\partial s}\right)\right]\left[\tfrac{\partial u}{\partial r}+\tfrac{R}{r+R}\tfrac{\partial v}{\partial s}-\tfrac{u}{r+R}\right],\\ q_w=-k\tfrac{\partial T}{\partial r}. \end{aligned}\right\} \tag{38}$$

Finally we arrive

$$\left.\begin{aligned} C_{fs}\mathrm{Re}^{0.5}=\tfrac{2}{1+\lambda_1}\left[f''(0)-\tfrac{f'(0)}{K}+\beta\left(\begin{array}{c} f'(0)f''(0)-\tfrac{1}{K}(f'(0))^2-f(0)f'''(0)\\ -\tfrac{1}{K^2}f(0)f'(0)-\tfrac{1}{K}f(0)f''(0) \end{array}\right)\right],\\ Nu_x\mathrm{Re}^{-0.5}=-\theta'(0), \end{aligned}\right\} \tag{39}$$

where $(\mathrm{Re})^{\frac{1}{2}}\left(=\sqrt{\tfrac{a}{\nu}}s\right)$ highlights the Reynolds number.

5. Entropy modeling

The entropy equation for the given flow is expressed as

$$\left.\begin{aligned} S'''_{gen}=\underbrace{\frac{k}{T_\infty^2}\left(\frac{\partial T}{\partial r}\right)^2}_{\text{heat transfer irreversibility}}+\underbrace{\frac{1}{T_\infty}\Phi}_{\text{viscous dissipation irreversibility}}+\underbrace{\frac{R_g D}{C_\infty}\left(\frac{\partial C}{\partial r}\right)^2+\frac{R_g D}{T_\infty}\left(\frac{\partial C}{\partial r}\frac{\partial T}{\partial r}\right)}_{\text{mass transfer irreversibility}}\\ +\underbrace{\frac{\sigma B_0^2 u^2}{T_\infty}}_{\text{Joule heating irreversibility}} \end{aligned}\right\} \tag{40}$$

where the Φ is defined as

$$\Phi = \frac{\mu}{1+\lambda_1}\left[\left(\frac{\partial u}{\partial r}\right)^2 - \frac{u}{r+R}\frac{\partial u}{\partial r} + \left(\frac{u}{r+R}\right)^2 + \lambda_2\begin{pmatrix} \frac{uv}{r+R}\frac{\partial^2 u}{\partial r^2} + \frac{uv}{(r+R)^2}\frac{\partial u}{\partial r} - \frac{u^2 v}{(r+R)^3} \\ -\frac{Ru^2}{(r+R)^2}\frac{\partial^2 u}{\partial r \partial s} + \frac{u^2 R}{(r+R)^3}\frac{\partial u}{\partial s} + v\frac{\partial u}{\partial r}\frac{\partial^2 u}{\partial r^2} \\ -\frac{v}{r+R}\left(\frac{\partial u}{\partial r}\right)^2 + \frac{uv}{(r+R)^2}\frac{\partial u}{\partial r} - \frac{uR}{(r+R)^2}\frac{\partial u}{\partial r}\frac{\partial u}{\partial s}\end{pmatrix}\right]\Bigg\}. \tag{41}$$

So we arrive

$$S'''_{gen} = \underbrace{\frac{k}{T_\infty^2}\left(\frac{\partial T}{\partial r}\right)^2}_{\text{heat transfer irreversibility}} + \underbrace{\frac{R_g D}{C_\infty}\left(\frac{\partial C}{\partial r}\right)^2 + \frac{R_g D}{T_\infty}\left(\frac{\partial C}{\partial r}\frac{\partial T}{\partial r}\right)}_{\text{mass transfer irreversibility}}$$
$$\Bigg\{\underbrace{\frac{1}{T_\infty}\frac{\mu}{1+\lambda_1}\left[\left(\frac{\partial u}{\partial r}\right)^2 - \frac{u}{r+R}\frac{\partial u}{\partial r} + \left(\frac{u}{r+R}\right)^2 + \lambda_2\begin{pmatrix} \frac{uv}{r+R}\frac{\partial^2 u}{\partial r^2} + \frac{uv}{(r+R)^2}\frac{\partial u}{\partial r} - \frac{u^2 v}{(r+R)^3} \\ -\frac{Ru^2}{(r+R)^2}\frac{\partial^2 u}{\partial r \partial s} + \frac{u^2 R}{(r+R)^3}\frac{\partial u}{\partial s} + v\frac{\partial u}{\partial r}\frac{\partial^2 u}{\partial r^2} \\ -\frac{v}{r+R}\left(\frac{\partial u}{\partial r}\right)^2 + \frac{uv}{(r+R)^2}\frac{\partial u}{\partial r} - \frac{uR}{(r+R)^2}\frac{\partial u}{\partial r}\frac{\partial u}{\partial s}\end{pmatrix}\right]}_{\text{viscous dissipation irreversibility}} + \underbrace{\frac{\sigma B_0^2 u^2}{T_\infty}}_{\text{Joule heating irreversibility}}\Bigg\}. \tag{42}$$

The dimensionless form is

$$N_G = \theta'^2\alpha_1 + MBrf'^2 + \frac{Br}{1+\lambda_1}\Bigg\{\begin{pmatrix} f'' - \frac{1}{\xi+K}f'f'' + \frac{f'^2}{(\xi+K)^2} \\ +\beta\begin{pmatrix} -\frac{K}{(\xi+K)^2}ff' - \frac{K}{(\xi+K)^3}ff'f'' + ff'^2\frac{K}{(\xi+K)^4} \\ -\frac{K}{(\xi+K)^2}f'^2f'' + f'^3\frac{K}{(\xi+K)^3}\end{pmatrix} \\ +L^*\theta'\phi' + L^*\frac{\alpha_2}{\alpha_1}\phi'^2\end{pmatrix}\Bigg\}. \tag{43}$$

Note that $Br\left(=\frac{\mu a^2 s^2}{k\Delta T}\right)$ indicates the Brinkman number, $\alpha_1\left(=\frac{\Delta T}{T_\infty}\right)$ the temperature difference parameter, $\alpha_2\left(=\frac{\Delta C}{C_\infty}\right)$ the concentration difference parameter, $L^*\left(=\frac{R_g D\Delta C}{k}\right)$ the diffusion parameter and $N_G\left(=\frac{S'''_{gen}T_\infty \nu}{k\Delta T a}\right)$ the entropy generation rate. Also note that R_g signifies the gas constant.

6. Results

Here numerical results are opted with the help of Built-in-Shooting technique for the nonlinear differential system (29)–(32) with boundary conditions (33) and compared the results with Sajid et al. [37] and Saif et al. [38]. Salient characteristics of pertinent flow parameters i.e., K, β, L_1, Nt, Nb, Pr, E_1, k_1, K, Br and λ_1 against $f'(\xi)$, $\theta(\xi), \phi(\xi)$, $N_G(\xi)$, Be, $C_{fs}\mathrm{Re}^{0.5}$ and $Nu_x\mathrm{Re}^{-0.5}$ are pointed out via Figs. 1–13 and Tables 1–2. Behavior of relaxation time (λ_1), Deborah number (β) and velocity slip parameter (L_1) against $C_{fs}\mathrm{Re}^{0.5}$ is addressed in Table 1. As anticipated, magnitude of $C_{fs}\mathrm{Re}^{0.5}$ diminishes against larger values of (λ_1), while it enhances via rising values of Deborah number. It is also noticed that magnitude of skin friction coefficient remain unchanged versus larger estimation of velocity slip parameter. Table 2 portrays Ec, Nt and Nb impacts on Nusselt number. Clearly, it is noticed that $Nu_x\mathrm{Re}^{-0.5}$ rises when Ec and Nt are increased whereas it declines against rising values of Brownian motion parameter. The comparative outcomes of present problem with Sajid et al. [37] and Saif et al. [38] is pointed out in Table 3. From Table 3, we see that our results are 100% matched with these studies. Fig. 1 portrays curvature parameter impact versus velocity field. We observed that velocity distribution reveals increasing trend subject to rising curvature parameter. Mathematically, curvature parameter is the ratio of stretching rate, radius and kinematic viscosity. Therefore, for larger curvature parameter, the radius of the surface increases due to which more fluid particles are sticked to the stretchable surface and consequently stretching rate increases. That is why velocity distribution increases. Fig. 2 exhibits Deborah number influence versus velocity distribution. Clearly, it is remarked that the velocity distribution displays diminishing trend against higher Deborah number. Deborah number is the

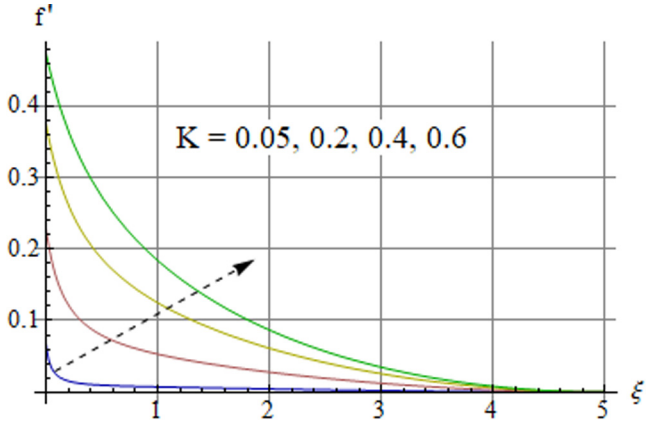

Fig. 1. K on $f'(\xi)$.

combination of retardation time and stretching rate. Therefore, for increasing the values of Deborah number, the retardation time of the material enhances which affect the velocity as well as the stretching rate of the material. Thus, velocity field is decreased. Outcome of velocity slip parameter on velocity distribution is highlighted in Fig. 3. As expected, the curves of velocity distribution dwindles against rising velocity slip parameter. In physical point of view, the deformation from the curved surface to the flowing fluid partially transfer subject to higher estimations of velocity slip parameter. Thus velocity distribution decays. Figs. 4 and 5 address Nt and Nb attributes versus temperature profile. As estimated, temperature profile boosts against rising Nt and Nb estimations. In physical point of view, Brownian motion is the random motion of working liquid particles on the surface. This pattern of liquid particles characteristically comprises of random oscillations in a particle's position inside a working liquid sub-domain, tracked by a replacement to another sub-domain. Each replacement is tracked by more oscillations within the new closed volume. The kinetic energies of the highly dense working liquid particles of molecular random motions, together with those of molecular vibrations and rotations, add up to the caloric component of the working liquid internal energy. Due to this fact, the temperature profile boosts. Influence of Prandtl number on temperature distribution is sketched in Fig. 6. It is inspected that temperature distribution and associated layer thickness declines versus rising Prandtl number. In fluid dynamics, boundary layer thickness is controlled by Prandtl number. Prandtl number is ratio of momentum diffusivity to thermal diffusivity. Thus for rising estimations of Prandtl number, the thermal diffusivity for the working fluid decays due to which temperature distribution diminishes. Fig. 7 reveals activation energy features versus concentration profile. Since activation energy marvel has a significant impact on concentration field. In this Fig., we observe that concentration profile rises when activation energy parameter is enhanced. Physically, the molecules or atoms of the working fluid store more energy through activation energy parameter and as a result the reaction between the fluid particles and nano-particles gets the higher rates. That is why the concentration profile boosts. The role of chemical reaction versus concentration profile in Fig. 8. Clearly, the mass concentration of nanoliquid declines against rising chemical reaction parameter. The concentration profile for various estimations of curvature parameter is evaluated versus Fig. 9. Here, nanofluid concentration boosts versus larger curvature variable. Physically, for larger curvature variable, the radius of curved surface upsurge due to which more fluid particles are sticked and as a result the mass diffusivity increases. Therefore, the concentration field is augmented. Figs. 10–13 are sketched to see how entropy generation rate and Bejan number affected by pertinent flow parameter. Figs. 10 and 11 are designed to elaborate variation in $N_G(\xi)$ and Be for distinct estimations of Brinkman number. Here, contrast behavior is remarked for $N_G(\xi)$ and Be against larger Brinkman number. Mathematically, Brinkman number is the combination of Prandtl number and Eckert number. Physically, for higher Brinkman number, the difference between the kinetic energy and boundary layer enthalpy enhances due to which more disorder occur in the working liquid and as a result entropy rate boosts. Behavior of relaxation time parameter against $N_G(\xi)$ and Be are displayed in Figs. 12 and 13. Here, dual behavior of both $N_G(\xi)$ and Be is noticed against larger relaxation parameter. Initially both $N_G(\xi)$ and Be decline versus relaxation parameter and then both profiles boost against larger relaxation parameter.

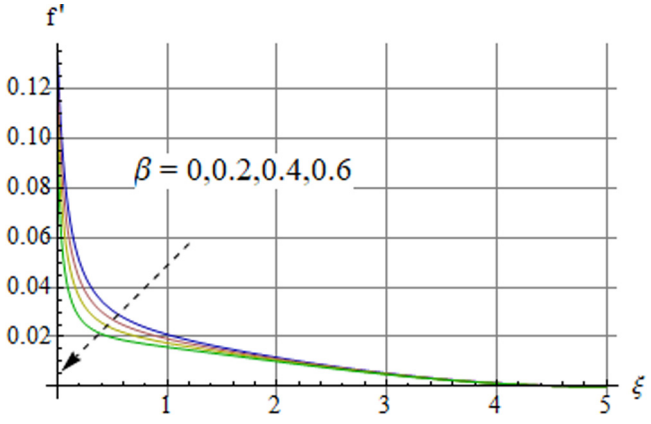

Fig. 2. β on $\left(f'(\xi)\right)$.

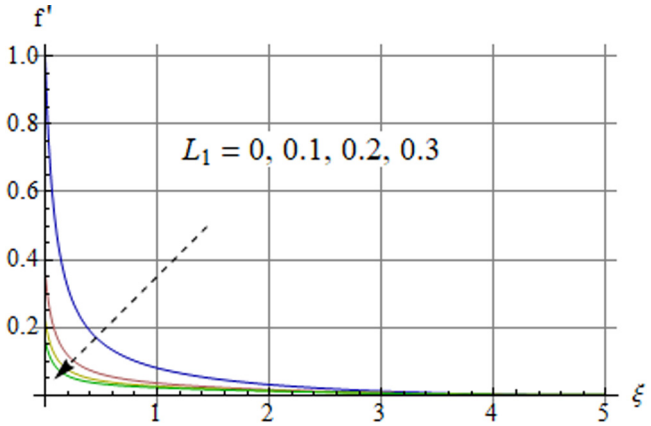

Fig. 3. L_1 on $\left(f'(\xi)\right)$.

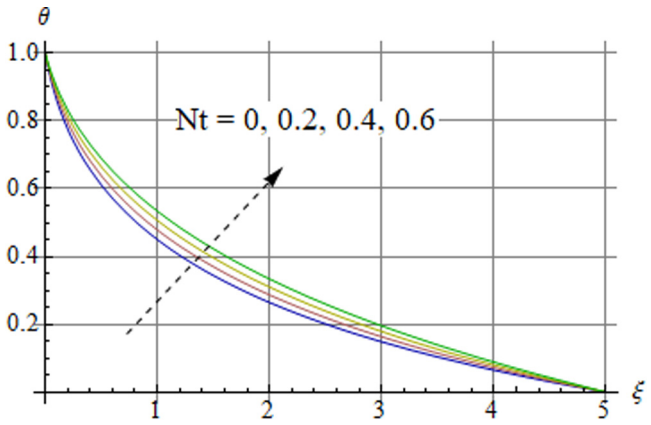

Fig. 4. Nt on $(\theta(\xi))$.

7. Conclusions

In this problem, mathematical modeling is designed for steady magnetized two-dimensional (2D) incompressible flow of Jeffrey nanofluid subject to curved surface. Velocity slip condition is further imposed on the curved

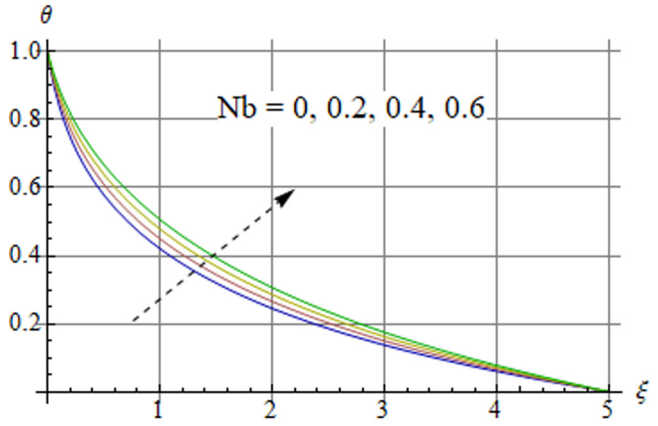

Fig. 5. Nb on $(\theta(\xi))$.

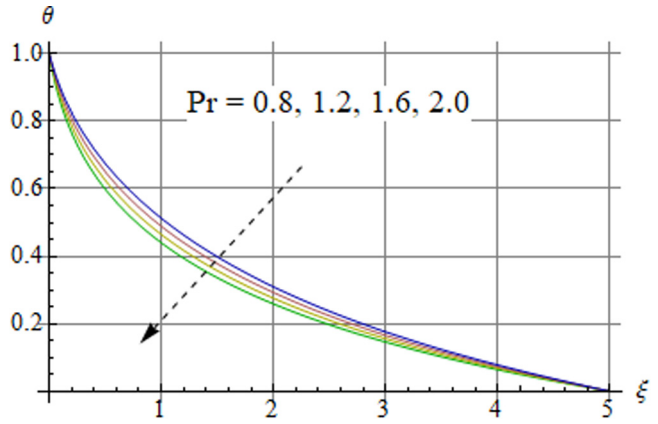

Fig. 6. Pr on $(\theta(\xi))$.

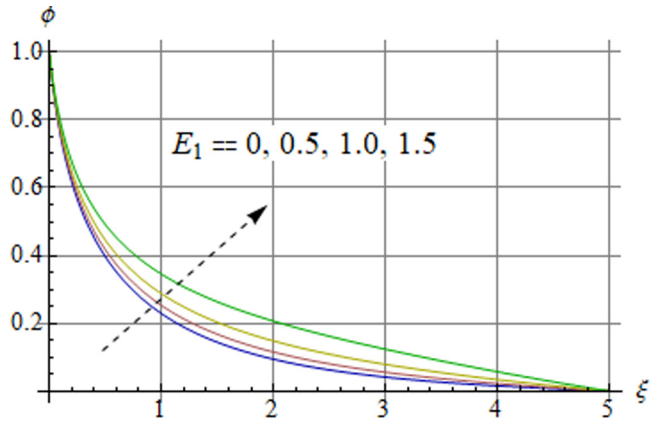

Fig. 7. E_1 on $(\phi(\xi))$.

stretched boundary. Total entropy generation rate which depends on the velocity, temperature and concentration fields is obtained via second law of thermodynamics. The dimensional differential equations are altered into the dimensionless ordinary differential system by using appropriate similarity variables. The salient characteristics

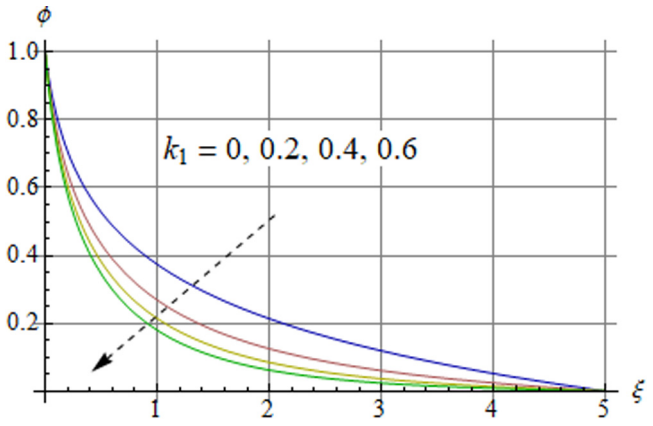

Fig. 8. k_1 on $\phi(\xi)$.

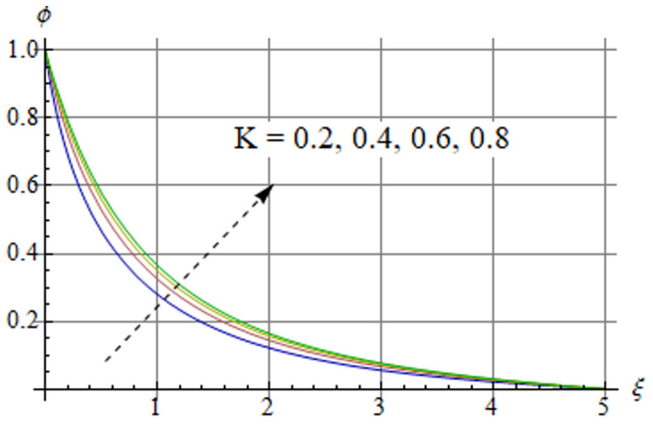

Fig. 9. K on $\phi(\xi)$.

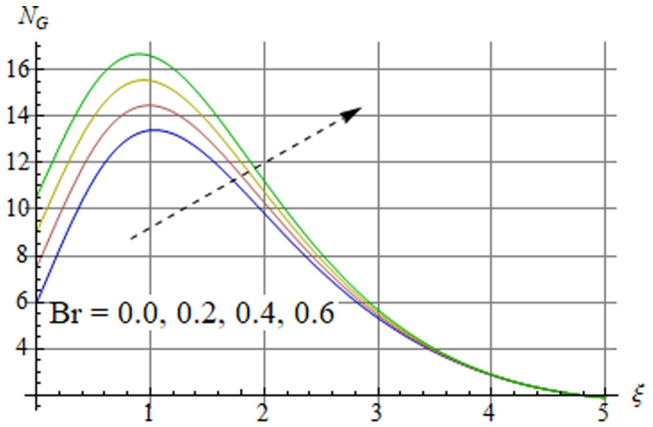

Fig. 10. Br on $N_G(\xi)$.

of flow parameters like curvature parameter, velocity slip parameter, Deborah number, thermophoresis diffusion, Prandtl number, Brownian motion, chemical reaction, Brinkman number and activation energy are sketched graphically for entropy generation rate, concentration, temperature and velocity field. It is observed from the obtained outcomes that the velocity distribution is greatly affected by the curvature parameter. Velocity distribution

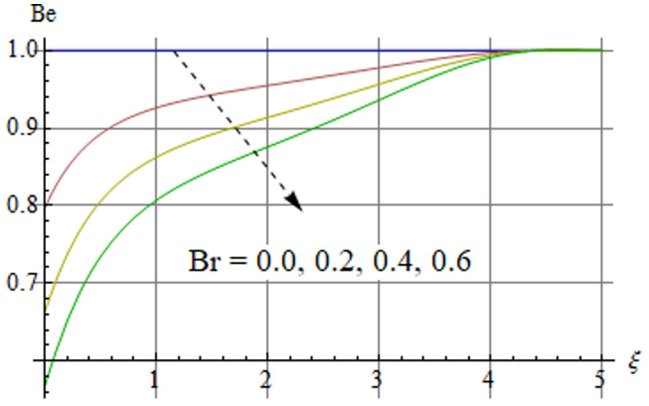

Fig. 11. Br on Be.

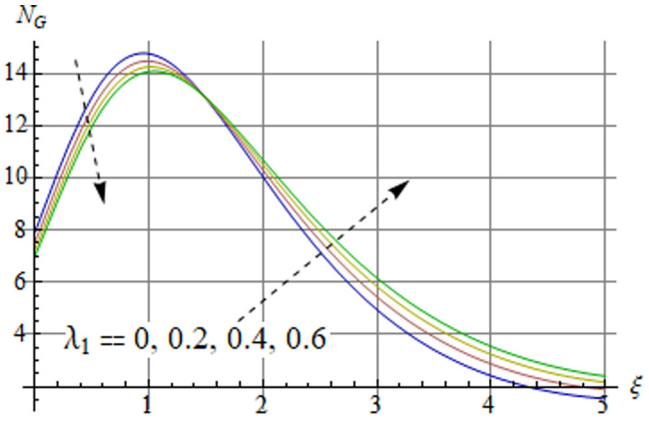

Fig. 12. λ_1 on $N_G(\xi)$.

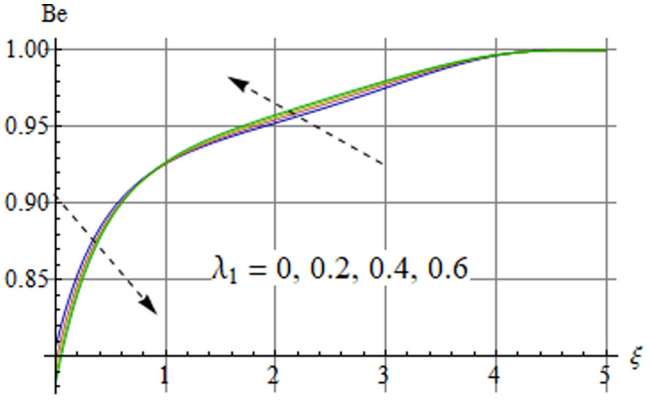

Fig. 13. λ_1 on Be.

is an increasing function of curvature parameter, while contrast impact is observed for Deborah number and velocity slip parameter. Temperature and concentration fields are increased versus Brownian motion, thermophoresis parameter, activation energy and curvature parameter respectively. It is also seen that the magnitude of skin friction upsurges versus the Deborah number while decays against relaxation time. Nusselt number is increased via larger Eckert number and declines against thermophoretic parameter.

Table 1
Examination of skin friction versus relaxation time parameter, Deborah number and velocity slip parameter.

λ_1	β	L_1	Skin friction
0.2	0.1	0.4	−4.33906
0.3			−4.2951
0.4			−4.25251
0.2	0.2		−4.34761
	0.3		−4.36042
	0.1	0.5	−3.02134
		0.6	−3.02134

Table 2
Examination of Nusselt number versus Brownian motion, Eckert number and thermophoresis.

Ec	Nt	Nb	Nusselt number
0.2	0.1	0.5	1.67259
0.3			1.68165
0.4			1.69071
0.2	0.2		1.56846
	0.3		1.47063
	0.2	0.6	1.54624
		0.7	1.42758

Table 3
Comparison of present work with previous study [37,38] when $\lambda_1 = \beta = L_1 = M = \lambda^* = N^* = \beta_t = \beta_c = 0$.

A	$f''(0) - \frac{1}{A} f'(0)$ [37]	$f''(0) - \frac{1}{A} f'(0)$ [38]	$f''(0) - \frac{1}{A} f'(0)$ [Present]
5	0.75781	0.75763	0.75759
10	0.87353	0.87349	0.87351
20	0.93572	0.93561	0.93559
30	0.95694	0.95686	0.95682

Data availability statement

The data that support the findings of this study are available within the article, the data are made by the authors themselves and do not involve references of others.

References

[1] A. Bejan, Second law analysis in heat transfer, Energy 5 (1980) 721–732.
[2] P.K. Singh, K.B. Anoop, T. Sundararajan, S.K. Das, Entropy generation due to flow and heat transfer in nanofluids, Int. J. Heat Mass Transfer 53 (2010) 4757–4767.
[3] O. Mahian, A. Kianifar, C. Kleinstreuer, A. Al-Nimr Moh'd, I. Pop, A.Z. Sahin, S. Wongwises, A review of entropy generation in nanofluid flow, Int. J. Heat Mass Transfer 65 (2013) 514–532.
[4] A. Ebrahimi, F. Rikhtegar, A. Sabaghan, E. Roohi, Heat transfer and entropy generation in amicrochannel with longitudinal vortex generators using nanofluids, Energy 101 (2016) 190–201.
[5] M.L. Sirisha, P. Dhar, Consequences of flow configuration and nanofluid transport on entropy generation in parallel microchannel cooling systems, Int. J. Heat Mass Transfer 109 (2017) 555–563.
[6] T. Hayat, M.I. Khan, S. Qayyum, A. Alsaedi, Entropy generation in flow with silver and copper nanoparticles, Colloids Surf. A 539 (2018) 335–346.
[7] E. Manay, E.F. Akyürek, B. Sahin, Entropy generation of nanofluid flow in a microchannel heat sink, Results Phys. 9 (2018) 615–624.
[8] Z. Xie, Y. Jian, Entropy generation of magnetohydrodynamic electroosmotic flow in two-layer systems with a layer of non-conducting viscoelastic fluid, Int. J. Heat Mass Transfer 127 (2018) 600–615.
[9] F. Shah, M.I. Khan, T. Hayat, M.I. Khan, W.A. Khan, Theoretical and mathematical analysis of entropy generation in fluid flow subject to aluminum and ethylene glycol nanoparticles, Comput. Methods Programs Biomed. 182 (2019) 105057.
[10] S. Ahmad, M.I. Khan, T. Hayat, M.I. Khan, A. Alsaedi, Entropy generation optimization and unsteady squeezing flow of viscous fluid with five different shapes of nanoparticles, Colloids Surf. A 554 (2018) 197–210.

[11] M. Torabi, M. Torabi, M.E. Yazdi, G.P. Peterson, Fluid flow, heat transfer and entropy generation analyses of turbulent forced convection through isotropic porous media using RANS models, Int. J. Heat Mass Transfer 132 (2019) 443–461.
[12] M.I. Khan, S. Kadry, Yu-Ming Chu, M. Waqas, Modeling and numerical analysis of nanoliquid (titanium oxide, Graphene oxide) flow viscous fluid with second order velocity slip and entropy generation, Chin. J. Chem. Eng. (2020) In press.
[13] R. Muhammad, M.I. Khan, N.B. Khan, M. Jameel, Magnetohydrodynamics (MHD) radiated nanomaterial viscous material flow by a curved surface with second order slip and entropy generation, Comput. Methods Programs Biomed. 189 (2020) 105294.
[14] M. Bahiraei, N. Mazaheri, M.R. Daneshyar, CFD analysis of second law characteristics for flow of a hybrid biological nanofluid under rotary motion of a twisted tape: Exergy destruction and entropy generation analyses, Powder Technol. 372 (2020) 351–361.
[15] R. Muhammad, M.I. Khan, M. Jameel, N.B. Khan, Fully developed Darcy-Forchheimer mixed convective flow over a curved surface with activation energy and entropy generation, Comput. Methods Programs Biomed. 188 (2020) 105298.
[16] T. Hayat, S.A. Khan, A. Alsaedi, Simulation and modeling of entropy optimized MHD flow of second grade fluid with dissipation effect, J. Mater. Res. Technol. 9 (2020) 11993–12006.
[17] M.I. Khan, F. Alzahrani, A. Hobiny, Z. Ali, Fully developed second order velocity slip Darcy-Forchheimer flow by a variable thicked surface of disk with entropy generation, Int. Commun. Heat Mass Transfer 117 (2020) 104778.
[18] N.T. Tayeb, K. Amar, K. Sofiane, L. Lakhdar, Thermal mixing performances of shear-thinning non-Newtonian fluids inside two-layer crossing channels micromixer using entropy generation method: Comparative study, Chem. Eng. Proc. Process Intensif. 156 (2020) 108096.
[19] S.A. Khan, T. Hayat, M.I. Khan, A. Alsaedi, Salient features of Dufour and Soret effect in radiative MHD flow of viscous fluid by a rotating cone with entropy generation, Int. J. Hydrog. Energy 21 (2020) 14552–14564.
[20] J.M. Avellaneda, F. Bataille, A. Toutant, G. Flamant, Variational entropy generation minimization of a channel flow: Convective heat transfer in a gas flow, Int. J. Heat Mass Transfer 160 (2020) 120168.
[21] L.J. Crane, Flow past a stretching plate, Z. Angew. Math. Mech. 21 (1970) 645–647.
[22] B.C. Sakiadis, Boundary-layer behaviour on continuous solid surfaces: I. Boundary-layer equations for two-dimensional and axisymmetric flow, AIChE J. 7 (1961) 26–28.
[23] P.S. Gupta, A.S. Gupta, Heat and mass transfer on a stretching sheet with suction and blowing, Can. J. Chem. Eng. 55 (1977) 744–746.
[24] Y.Y. Lok, N. Amin, I. Pop, Non-orthogonal stagnation point flow towards a stretching sheet, Int. J. Non-Linear Mech. 41 (2006) 622–627.
[25] M.S. Abel, M.M. Nandeppanavar, Heat transfer in MHD viscoelastic boundary layer flow over a stretching sheet with non-uniform heat source/sink, Commun. Nonlinear Sci. Numer. Simul. 14 (2009) 2120–2131.
[26] N.B.A. Ishak, I. Pop, Melting heat transfer in boundary layer stagnation-point flow towards a stretching/shrinking sheet, Phys. Lett. A 374 (2010) 4075–4079.
[27] J. Bao, Q. Yang, Bifurcation analysis of the generalized stretch-twist-fold flow, Appl. Math. Comput. 229 (2014) 16–26.
[28] M. Turkyilmazoglu, Extending the traditional Jeffery–Hamel flow to stretchable convergent/divergent channels, Comput. Fluids 100 (2014) 196–203.
[29] X. Si, L. Li, L. Zheng, X. Zhang, B. Liu, The exterior unsteady viscous flow and heat transfer due to a porous expanding stretching cylinder, Comput. Fluid 105 (2014) 280–284.
[30] M. Mustafa, J.A. Khan, T. Hayat, A. Alsaedi, On Bödewadt flow and heat transfer of nanofluids over a stretching stationary disk, J. Mol. Liq. 211 (2015) 119–125.
[31] Y.M. Chu, M.I.U. Rehman, M.I. Khan, S. Nadeem, S. Kadry, Z. Abdelmalek, N. Abbas, Transportation of heat and mass transport in hydromagnetic stagnation point flow of Carreau nanomaterial: Dual simulations through Runge–Kutta Fehlberg technique, Int. Commun. Heat Mass Transfer 118 (2020) 104858.
[32] M. Mustafa, J.A. Khan, T. Hayat, A. Alsaedi, Buoyancy effects on the MHD nanofluid flow past a vertical surface with chemical reaction and activation energy, Int. J. Heat Mass Transfer 108 (2017) 1340–1346.
[33] M. Awais, S. Saleem, T. Hayat, S. Irum, Hydromagnetic couple-stress nanofluid flow over a moving convective wall: OHAM analysis, Acta Astronaut. 129 (2016) 271–276.
[34] T. Hayat, S. Ayub, A. Alsaedi, B. Ahmad, Numerical simulation of buoyancy peristaltic flow of Johnson-Segalman nanofluid in an inclined channel, Results Phys. 9 (2018) 906–915.
[35] M.I. Khan, F. Alzahrani, Activation energy and binary chemical reaction effect in nonlinear thermal radiative stagnation point flow of Walter-B nanofluid: Numerical computations, Int. J. Mod. Phys. B 34 (2020) 2050132.
[36] M.I. Khan, M. Waqas, T. Hayat, A. Alsaedi, A comparative study of Casson fluid with homogeneous-heterogeneous reactions, J. Colloid Interface Sci. 498 (2017) 85–90.
[37] M. Sajid, N. Ali, T. Javed, Z. Abbas, Stretching a curved surface in a viscous fluid, Chin. Phys. Lett. 27 (2010) 024703.
[38] R.S. Saif, T. Muhammad, H. Sadia, R. Ellahi, Hydromagnetic flow of Jeffrey nanofluid due to a curved stretching surface, Physica A 551 (2020) 124060.
[39] T. Hayat, S. Qayyum, M. Imtiaz, A. Alsaedi, Jeffrey fluid flow due to curved stretching surface with Cattaneo-Christov heat flux, Appl. Math. Mech. 39 (2018) 1173–1186.
[40] M. Imtiaz, T. Hayat, A. Alsaedi, MHD convective flow of Jeffrey fluid due to a curved stretching surface with homogeneous-heterogeneous reactions, Plos One 11 (2016) e0161641.
[41] J. Harris, Rheology and Non-Newtonian Flow, Longman, London, 1977.
[42] H. Schichting, Boundary Layer Theory, sixth ed., McGraw-Hill, New York, 1964.